Topographic control of lipid-raft reconstitution in model membranes

TAE-YOUNG YOON[1]*, CHERLHYUN JEONG[1], SANG-WOOK LEE[1], JOON HEON KIM[2], MYUNG CHUL CHOI[2], SUNG-JIN KIM[1], MAHN WON KIM[2] AND SIN-DOO LEE[1]†

[1]School of Electrical Engineering #032, Seoul National University, Kwanak PO Box 34, Seoul 151-600, South Korea
[2]Department of Physics, Korea Advanced Institute of Science and Technology, 373-1, Gusong-dong, Yusong-gu, Daejon 305-701, South Korea
*Present address: Department of Physics, University of Illinois, Urbana-Champaign, Urbana, Illinois 61801, USA
†e-mail: sidlee@plaza.snu.ac.kr

Published online: 26 March 2006; doi:10.1038/nmat1618

Liquid-ordered (L_O) domains reconstituted in model membranes[1–6] have provided a useful platform for *in vitro* studies of the lipid-raft model[7–9], in which signalling membrane molecules are thought to be compartmentalized in sphingolipid- and cholesterol-rich domains. These *in vitro* studies, however, have relied on an uncontrolled phase-separation process that gives a random distribution of L_O domains. Obviously, a precise control of the size and spatial distribution of the L_O domains would enable a more systematic large-scale *in vitro* study of the lipid-raft model. The prerequisite for such capability would be the generation of a well-defined energy landscape for reconstituting the L_O domain without disrupting the two-dimensional (2D) fluidity of the model membrane. Here we report controlling the reconstitution of the L_O domains in a spatially selective manner by predefining a landscape of energy barriers using topographic surface modifications. We show that the selective reconstitution spontaneously arises from the 2D brownian motion of nanoscale L_O domains and signalling molecules captured in these nanodomains, which in turn produce a prescribed, concentrated downstream biochemical process. Our approach opens up the possibility of engineering model biological membranes by taking advantage of the intrinsic 2D fluidity. Moreover, our results indicate that the topographic configuration of cellular membranes could be an important machinery for controlling the lipid raft *in vivo*.

Our concept of topographically controlling the L_O domain formation is illustrated in Fig. 1. In a supported membrane system[10], the L_O domains and individual molecules that are smaller than about 10 nm show significant 2D dynamics whereas the L_O domains with physical dimension (d) larger than about 10 nm are practically immobilized because of friction with the solid support[10,11]. We call these small dynamic L_O domains 'nanorafts' and note that these are conceptually similar to previously suggested lipid shells[9] and condensed complexes[12]. The formation of mesoscopic or macroscopic L_O domains ($d \geq 10$ nm) in a supported membrane is thus made through coarsening of these nanorafts. Manipulating this coarsening process is essential for controlling the L_O domain formation in the supported membrane system.

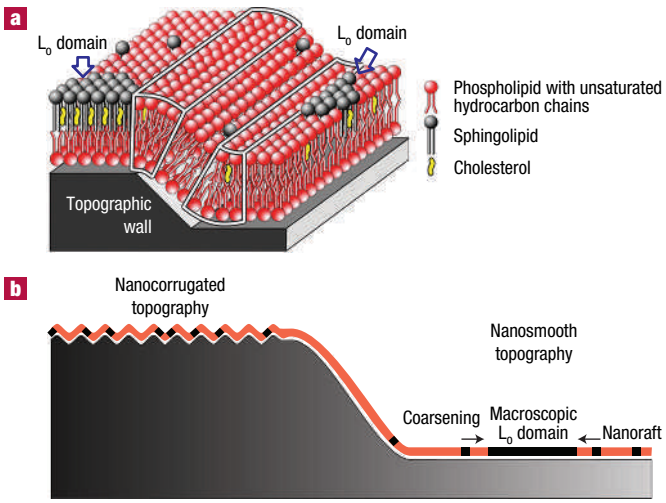

Figure 1 Schematic of the control of the reconstitution of L_O domains by topographic structures (not to scale). The supported membrane consists of the fluid background phase (mostly containing unsaturated phospholipids) and the L_O domains that are formed by association of sphingolipid and cholesterol molecules. **a**, The topographic wall produces elastic energy barriers at two edges (the white lines). The coarsening process of nanorafts is restricted by the elastic energy barriers. **b**, If the elastic energy barriers are integrated into the nanocorrugated topography, the coarsening of nanorafts and the resulting growth of L_O domains are confined in a region with nanosmooth topography.

Let us consider a supported membrane formed on a simple topographic structure, a topographic wall (Fig. 1a). The small contact curvature radius of the supported membrane (owing to

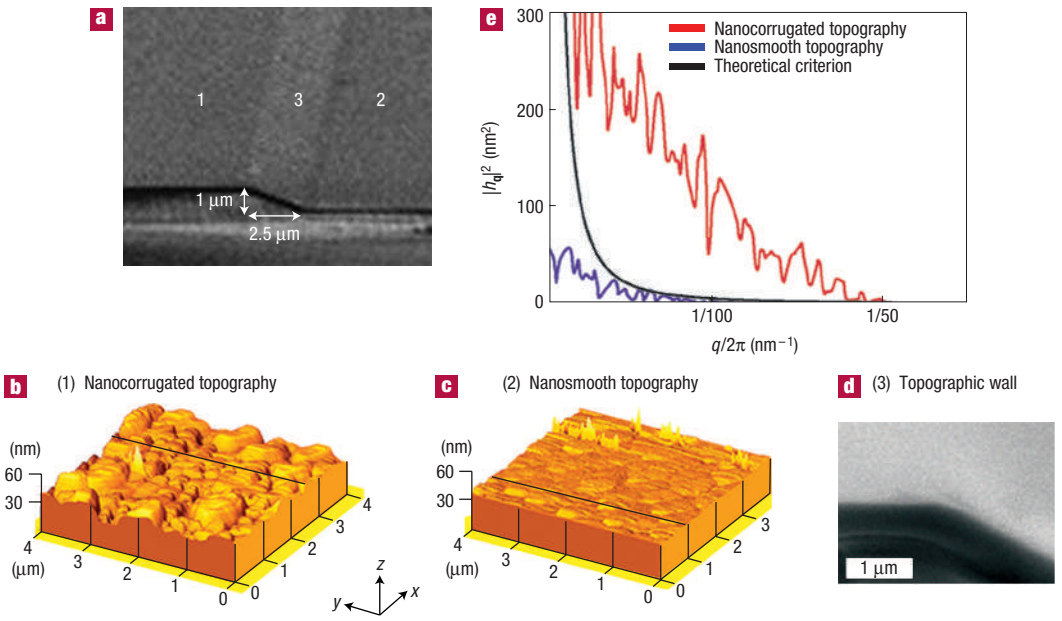

Figure 2 Solid support patterned to have different topographic structures. a, Scanning electron microscopy (SEM; XL30FEG, Philips) micrograph of the solid support. The labels 1, 2, and 3 denote different topographic structures: the nanocorrugated topography, the nanosmooth topography, and the topographic wall, respectively. **b**,**c**, Atomic force microscopy (AFM; AutoProbe CP, Park Scientific) measurements of the nanocorrugated topography (**b**) and the nanosmooth topography (**c**). **d**, Enlarged SEM micrograph of the topographic wall. **e**, Magnitude of $|h_{\mathbf{q}}|^2$ of the nanocorrugated topography (the red curve) and that of the nanosmooth topography (the blue curve). The Fourier components were measured along the dark lines in the AFM measurements of **b** and **c**. The theoretical boundary of coarsening due to the elastic energy barrier is represented by the black curve.

strong adhesion to the solid support)[13,14] causes the membrane to closely follow topographic structures. Elastic distortions of the supported membrane are then produced at predetermined positions, in this case, at the two edges shown in Fig. 1a as white lines. Under these elastic distortions, the L_O domains will have a larger free energy gain than the background fluid phase because of the larger bending rigidity (K_{L_o})[4–6] resulting from the tighter packing of the hydrocarbon chains[8,9]. This difference in the free-energy increase acts as an energy barrier that suppresses the coarsening process of nanorafts at the edges. The potential of this concept can be fully exploited by integrating the elastic energy barriers into a nanocorrugated topography (Fig. 1b). The coarsening process of nanorafts will be prohibited in the nanocorrugated region, and the formation of macroscopic L_O domains will then be confined in the nanosmooth region.

To describe our concept more quantitatively, the elastic energy barrier is represented as the Helfrich-type free energy[13,15], $(\Delta K d^2/2)\sum_{\mathbf{q}} q^4 |h_{\mathbf{q}}|^2$, in the 2D Fourier space of the wavevector $\mathbf{q} = (q_x, q_y)$. Here, ΔK denotes the difference in the rigidity coefficients, $K_{L_o} - K_{\mathrm{fluid}}$ (K_{fluid} is the bending rigidity of the fluid phase), $|\mathbf{q}| = q$, and $h_{\mathbf{q}}$ is the Fourier component of the topographic structure. The gaussian and the spontaneous curvatures are assumed to have negligible effects. In this Fourier space representation, each wavevector has an independent degree of freedom[13] and corresponds to a length scale of $2\pi/q$. Suppose that the energy barrier at $\mathbf{q}$ with $d = 2\pi/q$ becomes larger than thermal fluctuations of $k_B T$ (where k_B is Boltzmann's constant and T is temperature). In this situation, that is, the magnitude of $|h_{\mathbf{q}}|^2$ is larger than $(k_B T/8\pi^4 \Delta K)\cdot(q/2\pi)^{-2}$, the coarsening process of nanorafts will be limited on the length scale of $2\pi/q$. This means that the formation of L_O domains with the physical dimension of $d \geq 2\pi/q$ will be energetically unfavourable. This theoretical criterion for the coarsening process is plotted as a function of $q/2\pi$ in Fig. 2e (see the black solid curve). The magnitude of $\Delta K = 2.5 k_B T$, deduced from the measured value[16] of $K_{\mathrm{fluid}} = 10 k_B T$ and the ratio[4] of $K_{L_o}/K_{\mathrm{fluid}} = 1.25$, was used for our calculations. It is worth mentioning that the coarsening criterion for $|h_{\mathbf{q}}|^2$ would be larger if the line tension energy[4–6] that favours coarsening was taken into account.

On the basis of the predictions made above, we implemented different coarsening criteria into a solid support with various topographic structures, as shown in Fig. 2. The solid support consists of a SiO_2 layer (1.5 μm thick) formed on a (100) quartz wafer. For nanocorrugation, the tetraethoxysilane (TEOS) chemical vapour deposition method was used in forming the SiO_2 layer (Fig. 2b). The nanosmooth topography was obtained by chemically etching the nanocorrugated topography by 1 μm (Fig. 2c). Topographic walls were formed at the interfaces between the nanocorrugated and the nanosmooth regions (Fig. 2a,d). Note that our lithographic texturing is designed to alter only the surface topography. The solid support has a uniform surface chemistry of SiO_2 irrespective of the types of topographic structure (see Supplementary Information, Fig. S1).

As shown in Fig. 2e, $|h_{\mathbf{q}}|^2$ of the nanocorrugated topography (the red line in Fig. 2e) is much larger than the coarsening criterion in the range of $q/2\pi \leq 1/50$ nm^{-1}. In this case, the formation of the L_O domains with $d \geq 50$ nm will not be energetically favourable in the nanocorrugated region. In contrast, because the magnitude of $|h_{\mathbf{q}}|^2$ in the nanosmooth topography (the blue line in Fig. 2e) lies below the boundary in the whole range of $q/2\pi$, the formation of L_O domains will be promoted without physical limitations. Hence, the L_O domain formation will be confined within the nanosmooth region although the entire supported membrane contains nanorafts.

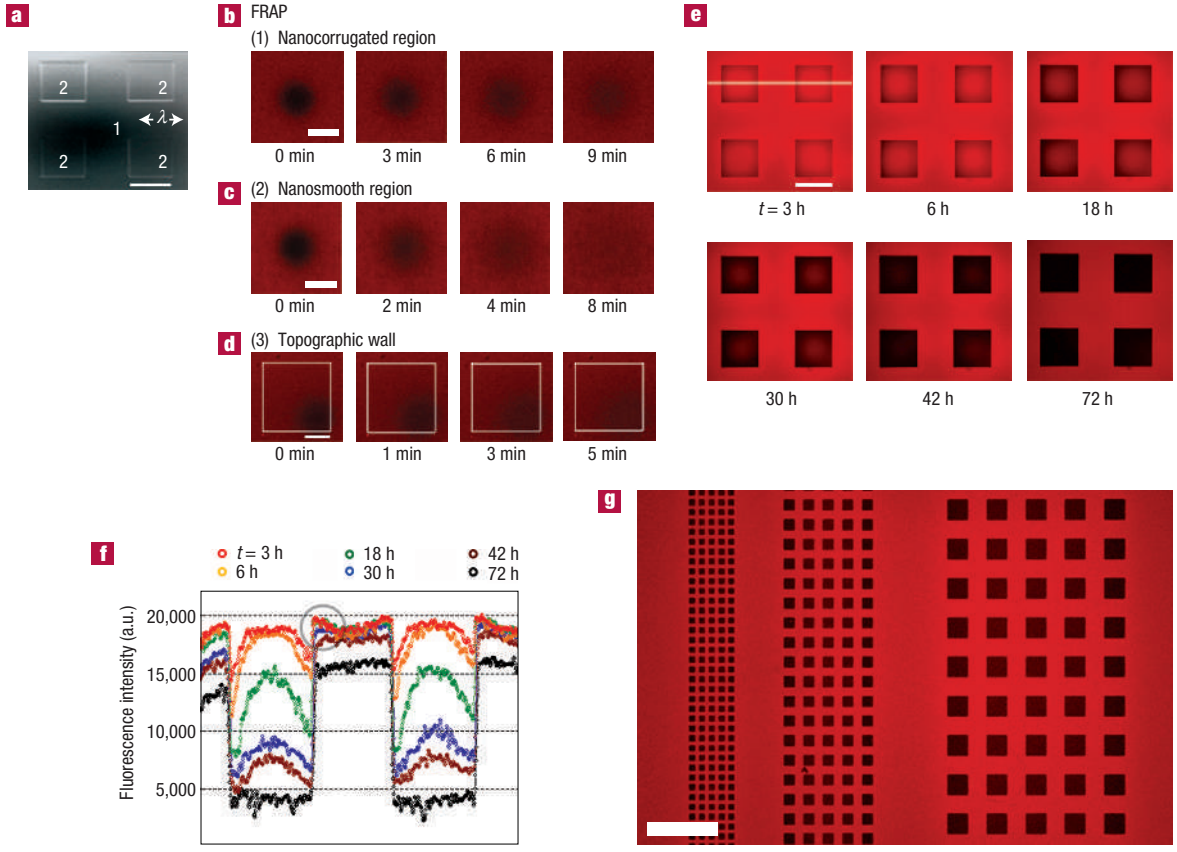

Figure 3 L_0 domain microarray. a, SEM micrograph of the solid support used for the L_0 domain microarray (the scale bar is 40 μm). The definitions of 1 and 2 are identical to those in Fig. 2. **b–d**, FRAP studies on the Texas red-DPPE molecules in the nanocorrugated topography (**b**, the scale bar is 40 μm), in one nanosmooth region (**c**, $\lambda = 200$ μm, the scale bar is 40 μm), and in the presence of topographic walls (the white lines) (**d**, $\lambda = 100$ μm, the scale bar is 40 μm). In particular, the fluorescence is recovered uniformly in all the azimuthal directions despite the presence of the topographic walls (the white lines of **d**), which indicates the lateral fluidity of the supported membrane across the topographic walls. Epifluorescence microscopy (Eclipse E600-POL, Nikon) was used in the Texas red channel. To minimize the decrease in the diffusion coefficients owing to the formation of macroscopic L_0 domains[1,6], the FRAP studies of **c** and **d** were carried out right after the vesicle fusion (within 20 min). **e**, Time evolution of the L_0 domain formation in an array of four nanosmooth regions ($\lambda = 200$ μm, the scale bar is 200 μm). The time $t = 0$ corresponds to the moment of the vesicle fusion. Epifluorescence microscopy was used in the Texas red channel. **f**, Time evolution of fluorescence intensity profiles. All of the profiles were measured along the white line of **e** at the corresponding time. In particular, the influx of nanorafts from the nanocorrugated background to the nanosmooth regions is reflected in the accumulation of Texas red-DPPE molecules at the boundaries of the nanocorrugated region (inside the grey circle). **g**, Epifluorescence micrograph of the L_0 domain microarray with λ values of 10 μm, 20 μm and 40 μm as observed in the Texas red channel ($t = 18$ h, the scale bar is 200 μm).

In light of the above idea, periodic arrays of nanosmooth regions (denoted by '2' in Fig. 3a) were created in a nanocorrugated background region (denoted by '1' in Fig. 3a) by a selective chemical etching process. The size of one nanosmooth region (λ) was varied from 3 μm to 200 μm. A supported membrane was produced on this solid support by the vesicle fusion method[17] at $t = 0$. The lipid composition used was the well-studied lipid-raft mixture[1–5] doped with Texas red 1,2-dihexadecanoyl-*sn*-glycero-3-phosphoethanolamine (Texas red-DPPE) and glycolipid G_{M1}. One important issue in our topographic control is that the 2D fluidity of the supported membrane should not be disrupted by the topographic structures. As a direct assessment, the fluorescence recovery after photo-bleaching (FRAP) studies[18] on the Texas red-DPPE molecules were carried out within individual topographic structures. Our FRAP studies indeed confirm that the 2D continuity and fluidity of the supported membrane are completely preserved in the nanocorrugated background (Fig. 3b, the diffusion coefficient of 1.06 $\mu m^2\ s^{-1}$), in one nanosmooth region of $\lambda = 200$ μm (Fig. 3c, the diffusion coefficient of 1.27 $\mu m^2\ s^{-1}$), and across the topographic walls (Fig. 3d).

As predicted, Fig. 3e shows that nanorafts coarsen and grow into macroscopic L_O domains only in the nanosmooth regions ($\lambda = 200$ μm). As the Texas red-DPPE molecules are strongly excluded from the L_O domains[1–3], the L_O domain formation can be monitored by the distribution of the red fluorescence from Texas red-DPPE. Importantly, the nanorafts initially present in the nanocorrugated background actively participate in the formation of L_O domains in the nanosmooth regions. This is clearly shown by the fact that the L_O domain formation is much faster at the boundaries than at the centre of each nanosmooth region (Fig. 3e,f). Using the 2D fluidity shown in Fig. 3b–d, when nanorafts that are kept from coarsening in the nanocorrugated background diffuse into a nanosmooth region, they begin to coarsen with other nanorafts. Such aggregated nanorafts are significantly hindered in their 2D brownian motion by the surface friction effect[13]. Thus, they are effectively trapped at the boundaries of the nanosmooth regions. This influx of nanorafts from the

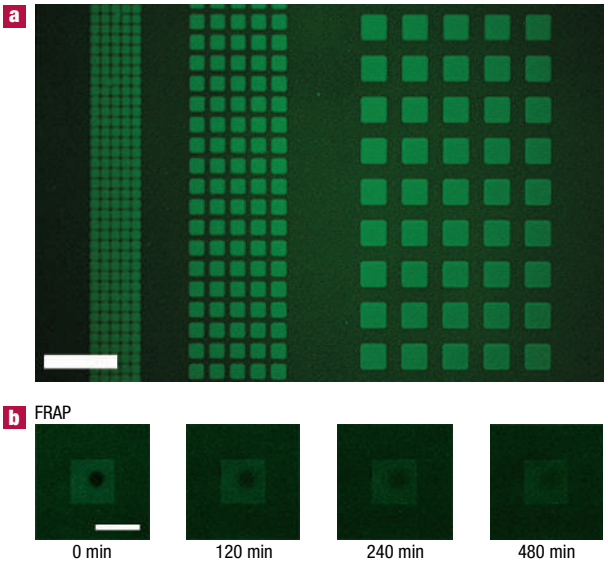

Figure 4 Selective reconstitution of the CTB–G_{M1} binding process in the L_O domain microarray. a, Epifluorescence micrograph of the L_O domain microarray of Fig. 3g, having been incubated with the Alexa Fluor 488-CTB, as observed in the Alexa Fluor 488 channel (the scale bar is 200 μm). **b**, FRAP study on the CTB–G_{M1} complexes ($\lambda = 40$ μm, the scale bar is 40 μm).

nanocorrugated background becomes saturated between $t = 42$ and 72 h in the case of $\lambda = 200$ μm (Fig. 3f). Furthermore, the L_O domain formation at the centre of the nanosmooth region is abruptly accelerated after about $t = 6$ h (Fig. 3f). As the coarsening process itself has no reasons for such acceleration, it is likely that the nanorafts previously trapped at the boundaries are effectively transported to the centre area. As a result, the final equilibrium state of the highly uniform L_O domain is reached at $t = 72$ h (Fig. 3e,f). It is observed that the time required for the equilibrium state decreases with the size of the nanosmooth region. For $\lambda \leq 40$ μm, the equilibrium state is attained earlier than $t = 18$ h (Fig. 3g). The topographic wall also plays a certain role in regulating the coarsening process, which is discussed in the Supplementary Information, Fig. S2.

In Fig. 3g, we show a microarray of the L_O domains, in which macroscopic L_O domains having different λ values of 10 μm, 20 μm and 40 μm are reconstituted in prescribed regions, the nanosmooth regions. It should be emphasized that this is the first time that model biological membranes have been engineered by taking advantage of the intrinsic 2D fluidity. No modifications of the typical supported membrane system are involved in controlling the L_O domain reconstitution except for the topographic structures.

We now show that a biochemical process with high affinity for the lipid raft acts selectively on the L_O domain microarray. The standard lipid-raft-marking process, the specific binding of cholera toxin unit B (CTB) to glycolipid receptor G_{M1} (ref. 19) was used as a model biochemical process. It is presumed that G_{M1} molecules that have high raft affinity are captured by the nanorafts[8,9] and show the same collective dynamics as the nanorafts (shown in Fig. 3e,f). Thus, the final equilibrium state will be a uniform concentrated distribution in each nanosmooth region, suggesting that the CTB–G_{M1} binding processes will predominantly occur in the nanosmooth regions.

Figure 4a shows the L_O domain microarray of Fig. 3g, which was incubated with a solution of Alexa Fluor 488-labelled CTB at $t = 180$ h. The strong green fluorescence in each nanosmooth region illustrates that the CTB–G_{M1} binding processes are highly concentrated in these preset regions. From the ratio of the green fluorescence in the nanosmooth regions to that in the nanocorrugated background, we obtained the partitioning coefficient of the CTB–G_{M1} binding process as approximately 2.28. The L_O domains with the CTB–G_{M1} complexes in the microarray show excellent temporal stability; they remained intact over 100 days (see Supplementary Information, Fig. S3). Moreover, the FRAP studies show that the CTB–G_{M1} complexes possess 2D fluidity with a diffusion coefficient of about 0.04 $\mu m^2\ s^{-1}$ (Fig. 4b). This result again leads to a definite conclusion that the domains reconstituted in the nanosmooth regions are indeed in an L_O phase, which has been essentially assumed in the lipid-raft model[7–9].

The approach described here offers a fundamental concept of organizing lipid rafts in model and cellular membranes. The paradigm of the lipid-raft model is being shifted from an image of a static huge domain to a concept that lipid rafts are extremely small and highly dynamic entities[20]. Then, there should be certain mechanisms for regulating coarsening of such extremely small lipid rafts and for tuning the kinetics of these lipid rafts to manipulate associated biochemical processes. We speculate that the nanoscale topographic configuration of the cellular membrane is one of the most important machineries for tuning lipid rafts *in vivo*. This machinery might provide a general pathway that translates a mechanical signal, that is, membrane curvature[21] to the biochemical processes that are mediated by the lipid raft.

METHODS

FABRICATION OF SOLID SUPPORTS

The solid support consists of a SiO_2 layer of 1.5 μm thick formed on a (100) quartz wafer. To produce a SiO_2 layer with the nanocorrugated topography shown in Fig. 2b, the TEOS chemical vapour deposition method using P-5000 (Applied Material Korea, South Korea) was used under the following conditions: (TEOS, O_2) = (220, 220) s.c.c.m., 9 torr and a deposition temperature of 390 °C. The resultant deposition rate was 125 Å s^{-1}. The nanosmooth topography as shown in Fig. 2c was obtained by chemically etching the nanocorrugated topography using buffered HF (7:1 (v/v) NH_4F:HF). The etching was carried out at room temperature without stirring, giving a resultant etching rate of approximately 1,000 Å min^{-1}. For the selective etching, the standard photolithography process was used, which produced the topographical structures shown in Fig. 2a. Owing to the small difference in the refractive index between SiO_2 and quartz (of the order of 10^{-3}), the interference effect occurring as a function of the SiO_2 layer thickness[22] is negligible.

FORMATION OF SUPPORTED MEMBRANES

The well-studied lipid-raft mixture, 1:1:1 (mol/mol/mol) 1,2-dioleoyl-*sn*-glycero-3-phophocholine:sphingomyelin (brain, porcine):cholesterol (all purchased from Avanti Polar Lipids, Birmingham, Alabama), was prepared, doped with a red fluorescent dye-labelled lipid, Texas red-DPPE (Molecular Probes, Eugene, Oregon) at 1 mol% of the total lipid composition. For the CTB–G_{M1} binding process, this lipid-raft mixture was further doped with ganglioside G_{M1} (brain, ovine-ammonium salt, Avanti Polar Lipids) at 1 mol%. All ingredients were dissolved in chloroform. To prevent demixing of cholesterols, the rapid solvent exchange method[23] was used, in which evaporation of solvent, desiccation and hydration processes were carried out simultaneously. The buffer contained 100 mM of NaCl and 10 mM of Tris at pH 8.0, and hydration was performed at a concentration of 0.2 mg ml^{-1}. Small unilamellar vesicles were obtained by the extrusion method (Mini-Extruder, Avanti Polar Lipids) with at least 60 filtering processes through a 50 nm filter at 50 °C. The solid support was cleaned in piranha solution (3:1 (v/v) H_2SO_4:H_2O_2) at 125 °C for more than 15 min before use in experiments. A supported membrane was produced by fusion of the small unilamellar vesicles on the solid support for more than 100 s at room temperature[22]. Excess vesicles were removed by changing the subphase from the vesicle suspension to

the phosphate buffer saline at pH 7.2, and this subphase was kept during the subsequent experiments.

CTB–G_{M1} BINDING PROCESS

For the CTB–G_{M1} binding process, the subphase of the G_{M1}-reconstituted lipid raft microarray was changed to a 5 μg ml^{-1} solution (in phosphate buffer saline at pH 7.2) of the Alexa Fluor 488 conjugated CTB (Alexa Fluor 488-CTB, Molecular Probes) for 75 min in the dark. During the binding process, the physiological temperature of 36.5 °C was maintained. After incubation, the subphase of the phosphate buffer saline at pH 7.2 was recovered.

Received 17 October 2005; accepted 24 February 2006; published 26 March 2006.

References

1. Dietrich, C. *et al.* Lipid rafts reconstituted in model membranes. *Biophys. J.* **80,** 1417–1428 (2001).
2. Dietrich, C., Volovyk, Z. N., Levi, M., Thompson, N. L. & Jacobson, K. Partitioning of Thy-1, GM1, and cross-linked phospholipids analogs into lipid rafts reconstituted in supported model membrane monolayers. *Proc. Natl Acad. Sci. USA* **98,** 10642–10647 (2001).
3. Veatch, S. L. & Keller, S. L. Organization in lipid membranes containing cholesterol. *Phys. Rev. Lett.* **89,** 268101 (2002).
4. Baumgart, T., Hess, S. T. & Webb, W. W. Imaging coexisting fluid domains in biomembrane models coupling curvature and line tension. *Nature* **425,** 821–824 (2003).
5. Roux, A. *et al.* Role of curvature and phase separation in lipid sorting and fission of membrane tubules. *EMBO J.* **24,** 1537–1545 (2005).
6. Bacia, K., Schwille, P. & Kurzchalia, T. Sterol structure determines the separation of phases and the curvature of the liquid-ordered phase in model membranes. *Proc. Natl Acad. Sci. USA* **102,** 3272–3277 (2005).
7. Simons, K. & Toomre, D. Lipid rafts and signal transduction. *Nat. Rev. Mol. Cell Biol.* **1,** 31–41 (2000).
8. Brown, D. A. & London, E. Structure and function of sphingolipid- and cholesterol-rich membrane rafts. *J. Biol. Chem.* **275,** 17221–17224 (2000).
9. Anderson, R. G. W. & Jacobson, K. A role for lipid shells in targeting proteins to caveolae, rafts, and other lipid domains. *Science* **296,** 1821–1825 (2002).
10. Sackmann, E. Supported membranes: scientific and practical applications. *Science* **271,** 43–48 (1996).
11. Kaizuka, Y. & Groves, J. T. Structure and dynamics of supported intermembrane junctions. *Biophys. J.* **86,** 905–912 (2004).
12. McConnell, H. M. & Radhakrishnan, A. Condensed complexes of cholesterol and phospholipids. *Biochim. Biophys. Acta* **1610,** 159–173 (2003).
13. Safran, S. A. *Statistical Thermodynamics of Surfaces, Interfaces, and Membranes* (Addison-Wesley, New York, USA, 1994).
14. Seifert, U. & Lipowsky, R. Adhesion of vesicles. *Phys. Rev. A* **42,** 4768–4771 (1990).
15. Helfrich, W. Elastic properties of lipid bilayers: theory and possible experiments. *Z. Naturforsch. C* **28,** 693–703 (1973).
16. Chen, Z. & Rand, R. P. The influence of cholesterol on phospholipid membrane curvature and bending elasticity. *Biophys. J.* **73,** 267–276 (1997).
17. Keller, C. A., Glasmästar, K., Zhdanov, V. P. & Kasemo, B. Formation of supported membranes from vesicles. *Phys. Rev. Lett.* **84,** 5443–5446 (2000).
18. Axelrod, D., Koppel, D. E., Schlessinger, J., Elson, E. & Webb, W. W. Mobility measurement by analysis of fluorescence photobleaching recovery kinetics. *Biophys. J.* **16,** 1055–1069 (1976).
19. Merritt, E. A. *et al.* Crystal structure of cholera toxin B-pentamer bound to receptor G_{M1} pentasaccharide. *Protein Sci.* **3,** 166–175 (1994).
20. Lin, J. & Shaw, A. S. Getting downstream without a raft. *Cell* **121,** 815–816 (2006).
21. McMahon, H. T. & Gallop, J. L. Membrane curvature and mechanisms of dynamic cell membrane remodelling. *Nature* **438,** 590–596 (2005).
22. Braun, D. & Fromherz, P. Fluorescence interferometry of neuronal cell adhesion on microstructured silicon. *Phys. Rev. Lett.* **81,** 5241–5244 (1998).
23. Buboltz, J. T. & Feigenson, G. W. A novel strategy for the preparation of liposomes: rapid solvent exchange. *Biochim. Biophys. Acta* **1417,** 232–245 (1999).

Acknowledgements

T.-Y.Y. thanks T. Ha and C.-J. Yu for valuable help and discussions, and M. K. Nahas, M. C. McKinney and B. Okumus for critical reading. This work was supported in part by the Korea Science and Engineering Foundation through the Center for Field Responsive Molecules at Korea University and Samsung SDI. M.W.K. acknowledges partial support from DMR-0080034, IMT-2000-B3-2, KISTEP I-03-064 and Korea Health 21 R&D Project of Republic of Korea.
Correspondence and requests for materials should be addressed to S.-D.L.
Supplementary Information accompanies this paper on www.nature.com/naturematerials.

Competing financial interests

The authors declare that they have no competing financial interests.